DOI: 10.1002/ejic.201001157

Structural, Magnetic and Dynamic Characterization of Liquid Crystalline Iron(III) Schiff Base Complexes with Asymmetric Ligands

Natalia Domracheva,*[a] Andrew Pyataev,[b] Rafil Manapov,[b] Matvey Gruzdev,[c] Ulyana Chervonova,[c] and Arkadij Kolker[c]

Keywords: Iron / EPR spectroscopy / Electronic structure / Molecular dynamics / Metallomesogens / Magnetic properties

The iron(III) complexes that were formed by coordination of the Fe^{III} ion with the asymmetric tridentate liquid crystalline Schiff base ligand (L), the water molecules and the different counterions [PF_6^- (**1**), NO_3^- (**2**), and Cl^- (**3**)] were studied by electron paramagnetic resonance (EPR) spectroscopy. EPR spectroscopy demonstrated that each of the complexes investigated consists of two types of iron centers: $S = 1/2$ low-spin (LS) and $S = 5/2$ high-spin (HS). LS iron complexes **2**, **3** and LS complex **1** in the temperature range 4.2–250 K have a $(d_{xz},d_{yz})^4(d_{xy})^1$ ground state. Interesting features were found for the monocationic Fe^{III} complex **1**, $[Fe(L)X(H_2O)_2]^+X^-$, with $X = PF_6^-$ as the counterion. The LS and HS iron centers of **1** are coupled together antiferromagnetically and form a dimer structure by means of the water molecules and the PF_6^- counterion. The second-type of LS and HS centers that are visible by means of EPR spectroscopy were best observed in the liquid crystalline (387–405 K) phase. The monitoring and the simulation of the EPR spectra enabled us to trace the dynamics of changing the number of the second-type of LS centers with respect to the first-type of LS centers. The observed dynamic process is characterized by the enthalpy value $\Delta H = 27.9$ kJ/mol, which was caused by reorientation of the PF_6^- counterion. Calculation of the observed g values for the second-type of LS complex **1** indicated that, in this case, the $(d_{xy})^2(d_{xz},d_{yz})^3$ ground state is stabilized. The conversion between the electron $(d_{xz},d_{yz})^4(d_{xy})^1/(d_{xy})^2(d_{xz},d_{yz})^3$ configurations was found to be temperature dependent and was detected in the same material for the first time in iron complexes.

Introduction

Six-coordinate d^5 Fe^{III} complexes with Schiff base ligands are known to display a variety of magnetic behaviors. Minor variations in all of the components of the complexes can lead to Fe^{III} high-spin ($S = 5/2$) or low-spin ($S = 1/2$) states and can also lead to spin-crossover behavior.[1–8] The design, synthesis, and characterization of iron complexes with Schiff base ligands has provided useful synthetic models for bioinorganic chemistry to mimic the active sites in iron-containing proteins and enzymes.[9–11] In particular, iron(III) complexes with salicylidene amine ligands serve as a structural and electronic model for the similarly coordinated iron(III) sites found in heme-iron enzymes.[12] One of the most important characteristics of these Schiff base ligands is that even small modifications of the structure can significantly change key properties of the corresponding iron complex.[9] For example, the introduction of several electron-withdrawing nitro groups into iron complexes with salen-type ligands led to effective catalysts for hydrocarbon oxidation with dioxygen as the oxidant.[13,14] It has been reported that the replacement of a methoxy group with an ethoxy group in a hexadentate N_2O_2 Schiff base ligand resulted in dramatic changes in the magnetic properties of the corresponding iron complexes due to small alterations in the intermolecular interactions and crystal packing.[15]

The motivation for this work arose from our desire to find a novel material based on iron(III) Schiff base complexes with asymmetric ligands that combined the liquid crystal properties (fluidity, easy processability, order) with those associated with metal atoms (magnetism, optics, conductivity). Future technological demands will require multifunctional materials where several different physical or chemical properties are exhibited in a single material. The liquid crystalline (LC) properties of our novel compounds were provided by the rod-like geometry, which was introduced by using elongated substituents in the Schiff base ligand.

A large number of six-coordinate iron(III) complexes with Schiff base ligands are known, but their liquid crystalline analogues have only been obtained comparatively recently. The first steps in the study of spin-crossover behavior for the bis(tridentate) Fe^{III} complexes that exhibit liquid

[a] Russian Academy of Science, Zavoisky Kazan Physical-Technical Institute,
Sibirsky Tract 10/7, 420029 Kazan, Russian Federation
Fax: +7-8432-725-075
E-mail: domracheva@mail.knc.ru
[b] Kazan Federal University,
Kremlyovskaya St. 18, 420008 Kazan, Russia
[c] Institute of Solution Chemistry,
Akademicheskaya St. 1, 153045 Ivanovo, Russia

Supporting information for this article is available on the WWW under http://dx.doi.org/10.1002/ejic.201001157 or from the author.

 © 2011 Wiley-VCH Verlag GmbH & Co. KGaA, Weinheim

crystalline properties were made in ref.[16,17]. The investigation of mono(tridentate) Fe^{III} Schiff base complexes with asymmetric ligands is in the early stages,[18] but their liquid crystalline analogues are unknown at the present time.

In this article we report on the study of iron(III) LC complexes with an asymmetric mono(tridentate) azomethene ligand (L), where L is azomethine 4,4′-dodecyloxybenzoyloxybenzoyl-4-salicyliden-*N*′-ethyl-*N*-ethylenediamine, and three different types of counterions, PF_6^-, NO_3^-, and Cl^-. All of the synthesized compounds were characterized by thin layer chromatography, elemental analysis, IR, and NMR spectroscopy.[19] The LC properties were studied by differential scanning calorimetry.[19] The presence of the complex-forming ion was confirmed by FTIR spectra in the far region.[20] The structure of the compounds, which was established by matrix-assisted laser desorption/ionization time of flight (MALDI-TOF), is in good agreement with the data obtained from elemental analysis. The iron(III) complexes are denoted as **1**, **2**, and **3** according to their counterions PF_6^-, NO_3^-, and Cl^-, respectively. The molecular structure of the complexes **2** and **3** was formed by coordination of a mono(tridentate) ligand (L), a water molecule and two counter anions [Fe(L)-$X_2(H_2O)$], where X = NO_3^- or Cl^-. Compound **1** is a monocationic mono(ligand) Fe^{III} complex, $[Fe(L)X(H_2O)_2]^+X^-$ where X = PF_6^-, in which the iron(III) ion has an octahedral configuration formed by three ligator (ONN) atoms of the tridentate ligand, one counterion and two water molecules (see Scheme 1).

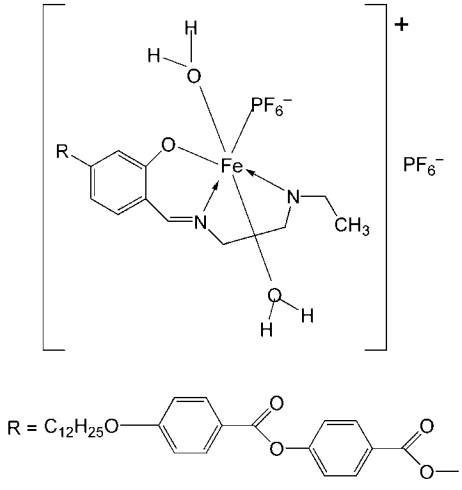

Scheme 1. Schematic representation of the structure for complex **1**, which is based on analogy to ref.[18]

Analogous coordination has been found in the research of Leovac [18] for a similar non-mesogenic iron(III) complex **30** with an asymmetric Schiff base ligand and the structure of complex **1** is based on analogy to ref.[18]

Results and Discussion

EPR Spectroscopy

Similar X-band EPR spectra (Figure 1) were observed for all of the compounds in the temperature range of 4.2 to 300 K and consisted of two types of signals: a low-field signal with $g_{eff.}$ = 4.3 that arose from the high-spin (HS) Fe^{III} ions and a high-field signal that corresponded to the low-spin (LS) Fe^{III} species. The magnetic parameters of these signals were independent of temperature. The EPR spectrum for the first type belonged to Fe^{III} ions that have the $^6S_{5/2}$ ground term and that are described by the spin Hamiltonian in Equation (1), where g = 2, S = 5/2. D and E are zero-field splitting parameters, which are induced by distortions of the crystal field in the compound.

$$\hat{H} = g\beta\hat{B}\hat{S} + D[\hat{S}_z^2 - \frac{1}{3}S(S+1)] + E(\hat{S}_x^2 - \hat{S}_y^2) \quad (1)$$

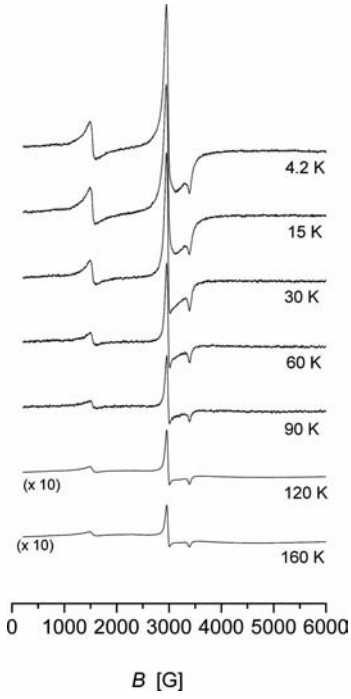

Figure 1. The EPR spectra of the polycrystalline complex **2** at different temperatures; ν = 9.47 GHz.

The observation of resonance at $g_{eff.}$ = 4.3 indicated[21] that the high-spin Fe^{III} ions have a strong ($D > h\nu$) low-symmetry ($E/D \approx 1/3$) crystal field ($h\nu$ is the microwave energy and is ca. 0.3 cm^{-1} at X-band frequencies). The EPR spectrum of the second type is typical of S = 1/2 Fe^{III} ions that have the $^2T_2$ (t_{2g}^5) ground term and that are described by the spin Hamiltonian of rhombic symmetry, see Equation (2), where the g values are close to 2. The observed g tensor values are given in Table 1. It should be noted, that the values found are typical of those found for the low-spin iron(III) complexes.[22–24a]

$$\hat{H} = \beta(g_x\hat{B}_x\hat{S}_x + g_y\hat{B}_y\hat{S}_y + g_z\hat{B}_z\hat{S}_z) \quad (2)$$

The calculation of the integrated EPR intensity for the HS and LS centers showed that the ratio between these cen-

 © 2011 Wiley-VCH Verlag GmbH & Co. KGaA, Weinheim

Table 1. Experimental and calculated EPR parameters for the LS iron(III) complexes.

Complex	g_x	g_y	g_z	A	B	C	k	Δ/λ	V/λ	$\Delta E_{12}/\lambda$	$\Delta E_{13}/\lambda$
1 (of the first-type)	–2.215	–2.215	1.935	0.1007	0.9939	0	0.848	2.677	0.007	7.662	8.597
1 (of the second-type)	1.975	–1.98	–2.165	0.7436	0.0005	0.6657	0.793	–5.506	1.489	8.984	21.056
1 (in N-8)	–2.209	–2.228	1.945	0.089	0.9951	0.003	0.954	2.866	0.107	8.123	9.259
2	–2.22	–2.23	1.948	0.0925	0.9954	0.0017	0.935	2.817	0.062	8.042	9.049
3	–2.225	–2.23	1.935	0.0936	0.9938	0.0008	0.9646	2.7989	0.0331	8.012	8.971
$Fe(L)_2PF_6$	–2.146	–2.233	1.969	0.0715	0.9973	0.0141	0.992	3.584	0.743	8.553	13.101

ters depends on the type of counterion (the fraction of the HS centers being minimal for Cl^- and maximal for PF_6^- counterions). However, the thermally driven spin-crossover transition from a spin state of $S = 1/2$ to a state of $S = 5/2$ was not detected for the compounds under investigation.

The samples changed behavior after two months of standing at ambient conditions. After ageing the appearance of a broad line (≈ 2000 G) was observed on a low-spin signal (Figure 2) for the iron complexes with the NO_3^- and Cl^- counterions.

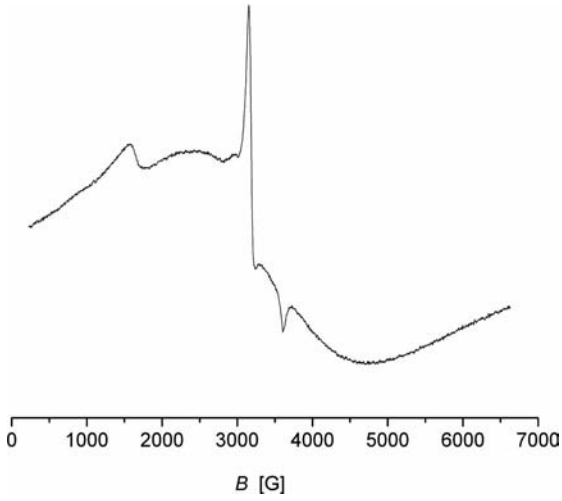

Figure 2. The room temperature EPR spectrum of complex **2** after ageing the complexes for two months.

The appearance of this broad line may be caused by iron cluster formation, since the NO_3^- counterion can form a bridge between the metal centers.[24b]

Compound **1** with the PF_6^- counterion behaves in a different way. The EPR spectra, together with the temperature dependence of their intensity for compound **1**, presented an exceptional case among the investigated iron complexes. These features will be considered below.

We first tried to assign the magnetic (principal) g axes to the molecular symmetry axes for the LS iron complex **1** since such information was unknown and crystals suitable for an X-ray structure determination could not be grown. For this purpose the method of orientation of paramagnetic molecules in the anisotropic solvent was used as described in ref.[25,26] The nematic liquid crystal (LC) N-8 (eutectic mixture: 4-methoxy- and 4-ethoxybenzylidene-4′-*n*-butylaniline) was employed as the anisotropic solvent. The investigated paramagnetic molecules have a rod-like geometry due to the elongated alkyl chains (tails). Such rod-like molecules are known to align in nematic liquid crystals along the director ***n*** (the characteristic direction of the sample orientation) owing to the interaction with the LC matrix of the elongated alkyl chains. Note, that the magnetic g tensor axes are mainly determined by the nearest neighbors of the iron ion (the distorted octahedron).

The orientation of the LS paramagnetic molecules was observed by sharply cooling a solution of complex **1** in the N-8 matrix in the presence of a high magnetic field (B_0 = 8000 G). The observed orientation, which is characterized by a director ***n***, is due to the field B_0. This is maintained when the sample freezes to the glassy state upon lowering the temperature. Thus, one can investigate the EPR line intensity dependence on the angle ξ between ***n*** and ***B*** by rotating the sample with respect to the external magnetic field. If the molecular y axis is oriented along ***n***, then the spectral line related to this axis of the complex has to be of maximal intensity for the initial orientation (ξ = 0°) and minimal intensity after rotation of the sample by 90°. Theoretical calculations [27] and experimental data[28] have also demonstrated that the EPR line intensity must have a maximum in the angular dependence at intermediate ξ values, if the magnetic axes of the g tensor and the molecular axes do not coincide.

The monotonic change of the EPR line intensities with the angle ξ variation (Figure 3, a) clearly shows that the direction of the molecular and the principal g tensor axes coincide. As seen in Figure 3 (a), the y component of the g tensor LS iron complex **1** decreases, and the z component increases when the sample is rotated through 90°. Such spectral features indicated that the molecular y axis was oriented along the director ***n***. For a qualitative analysis of the observed EPR spectra, we used the theory developed for paramagnetic probes in the oriented liquid crystals.[27,28] The EPR spectra were simulated by using a home-written program with algorithms described in ref.[27,28]. For nematic liquid crystals the orientational distribution function has an exponential form and is expressed as Equation (3), where ψ and ϕ are Euler angles that connect the molecular coordinate system and the sample coordinate system (determined by the director ***n***) and R_i ($i = x, y, z$) are the effective orientational parameters.

$$P(\psi,\varphi) \approx \exp(-R_x \sin^2\psi \sin^2\varphi - R_y \sin^2\psi \cos^2\varphi - R_z \cos^2\psi) \quad (3)$$

 © 2011 Wiley-VCH Verlag GmbH & Co. KGaA, Weinheim

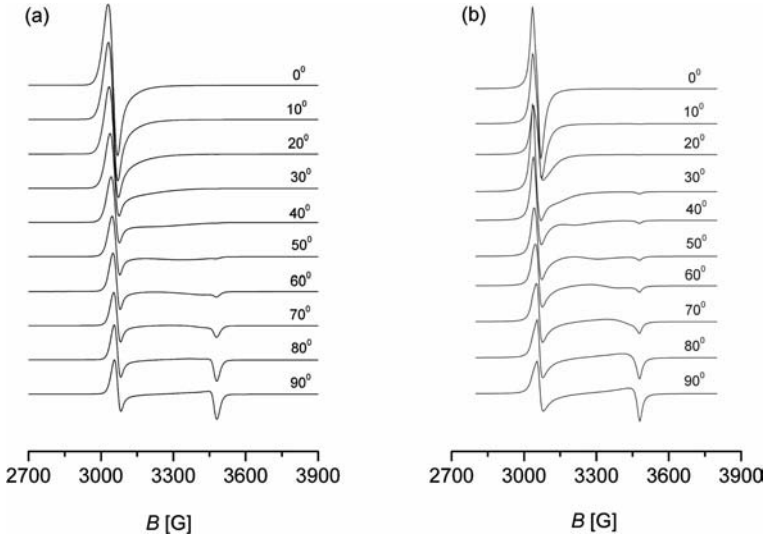

Figure 3. a) The experimental and b) the simulated EPR spectra for complex **1** at a low temperature in a eutectic mixture of N-8, which was previously oriented in the magnetic field (B_0 = 8000 G) for different angles ξ (a curve parameter).

Figure 3 (b) shows the simulated EPR spectra of the LS complex **1**, calculated with the following orientational parameters $R_y = 0$, $R_x = 6$, and $R_z = 7$ and magnetic parameters $g_x = 2.209$, $g_y = 2.228$, and $g_z = 1.945$. The individual Lorentzian line shape and line width of 15 G was used for the simulation. The degree of orientation of the molecular ($i = x, y, z$) axes of the LS complex **1** were $S_y = 0.71$, $S_x = -0.36$, and $S_z = -0.35$.

It is known that the mono(tridentate)-coordinated Schiff base ligand has an almost planar conformation from the structural data for a similar non-liquid-crystalline iron(III) complex **30** with an asymmetric Schiff base ligand.[18] Thus, based on the orientation results for the LS complex **1** in the nematic liquid crystal (N-8), we concluded that the long molecular *y* axis of the LS complex **1** lies in the (ONN) coordination plane and its direction is determined by the elongated alkyl tails, the *x* axis is perpendicular to *y* and also lies in this plane, while the molecular *z* axis is perpendicular to the (ONN) plane.

From the known crystal structure for the analogous non-liquid-crystalline complex **30**,[18] we were able to postulate that two water molecules occupy the *trans* position to the coordination (ONN) plane in the LS complex **1**, and that one PF_6^- counterion is ionically bound to the Fe^{III} ion and occupies the fourth position in this plane, whereas the other PF_6^- counterion lies in the second coordination shell.

Some interesting features of the polycrystalline complex **1** are detailed below. The EPR intensities of both the LS and the HS centers of complex **1**, which was obtained by numerical double integration, exhibit a significant temperature dependence with a maximum at $T_N \approx 7$ K (Figure 4, a). Above T_N the EPR integrated intensities follow the Curie–Weiss law with a paramagnetic Curie–Weiss constant $\theta_1 = -14.1$ K and $\theta_2 = -15.1$ K for the LS and the HS centers (Figure 4, b and c), respectively. The negative sign of θ indicates an antiferromagnetic coupling between the Fe^{III} ions. In accordance with the integrated intensity ratio, the number of LS to HS molecules is approximately 1:1. If we normalize the integrated intensity of each molecule fraction and superimpose these curves, identical magnetic behavior for the LS and the HS centers is observed (Figure 4, a). This shows that the LS and the HS iron(III) ions are coupled together and form a dimer structure, where the PF_6^- counterion and the water molecules are, probably, the bridging units.

Another interesting feature of complex **1** is the change in the number of low-spin (n_{LS}) molecules with respect to high-spin (n_{HS}) molecules with an increase in temperature. As seen in Figure 5 (a), the ratio only changes after 260 K when it begins to increase up to 340 K and then monotonically decreases to the melting point. The temperature dependence of increasing the number of n_{LS}/n_{HS} centers can be characterized by the equilibrium constant (K) and is described by Equation (4).

$$\ln K = \ln(n_{LS}/n_{HS}) = -\frac{\Delta H}{RT} + \frac{\Delta S}{R} \quad (4)$$

The thermodynamic parameters [enthalpy (ΔH) and entropy (ΔS)] of that process, $\Delta H = 0.76$ kJ/mol and $\Delta S = 0.0056$ kJ/mol, were calculated from the straight line given by plotting $\ln K$ vs. $1/T$ (Figure 5, b). The obtained enthalpy value is very small and is close to the energy needed for *cis*/*trans* isomerization position of the water molecules (0.42 kJ/mol), if the energy of these molecules changes only because the geometry of the compound changes.[29] Thus, we can assume that an increase in the number of LS centers to HS centers is likely to be caused by the transition of one water molecule from the axial (*trans*) position to the (*cis*) position in the coordination (ONN) plane.

The next important feature of complex **1** is the appearance of the second-type of LS center that is characterized by the magnetic parameters: $g_1 = 1.975$, $g_2 = 1.98$, and $g_3 = 2.165$. This new type of LS center is best observed in

 © 2011 Wiley-VCH Verlag GmbH & Co. KGaA, Weinheim

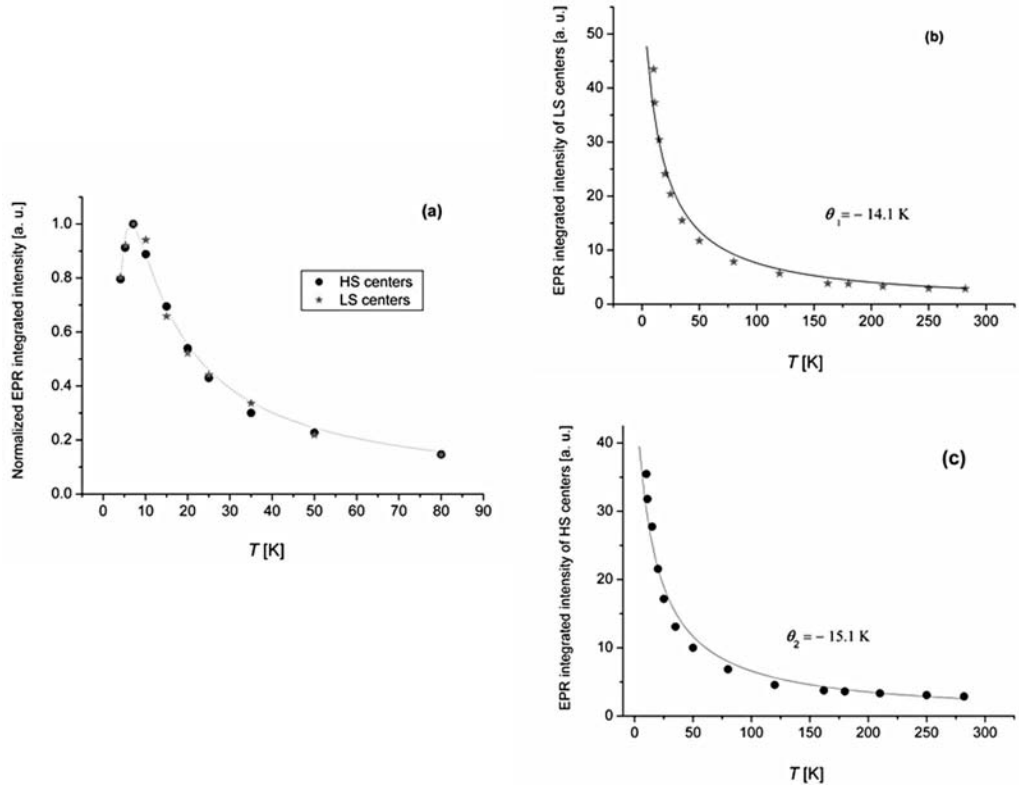

Figure 4. a) The temperature dependence (4.2 K ≤ T ≤ 80 K) of the EPR normalized integrated intensity of the HS and LS centers; b) the experimental (★) and the simulated (−) temperature dependence of the EPR integrated intensity of the LS centers at 9.5 K ≤ T ≤ 280 K. The solid line corresponds to the Curie–Weiss fit with θ_1 = –14.1 K; c) the experimental (·) and the simulated (−) temperature dependence of the EPR integrated intensity of the HS centers at 9.5 K ≤ T ≤ 280 K. The solid line corresponds to the Curie–Weiss fit with θ_2 = –15.1 K.

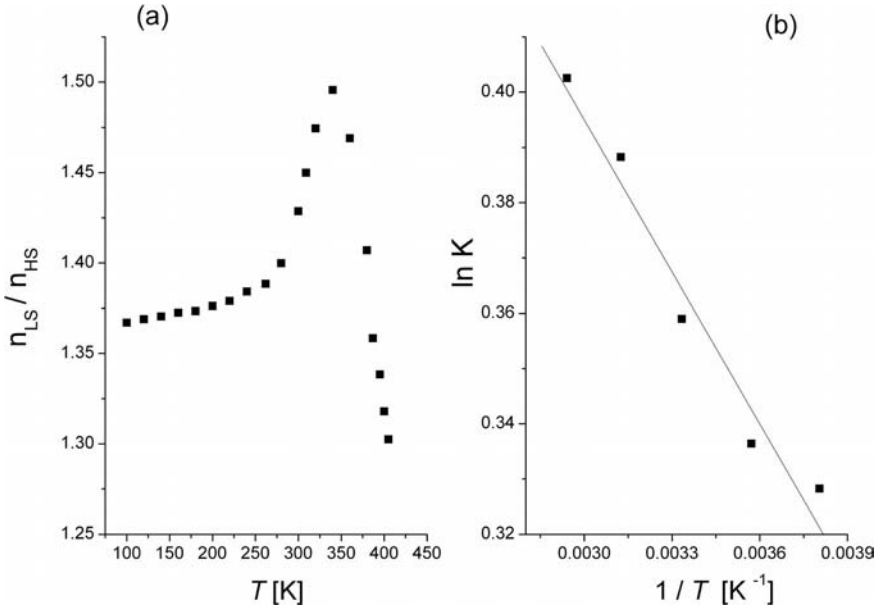

Figure 5. a) The temperature dependence of changing the number of LS/HS centers for complex **1**; b) ln K vs. 1/T for complex **1**. The solid line was calculated by means of Equation (4).

the liquid crystalline phase at high (387–405 K) temperature (Figure 6, b), but a small fraction of these centers are registered also at low temperature (Figure 6, a). The EPR spectra simulation enabled us to separate both types of LS signals and to trace the dynamics of changing the number of the second-type of LS centers (n_2) relative to the first ones

 © 2011 Wiley-VCH Verlag GmbH & Co. KGaA, Weinheim

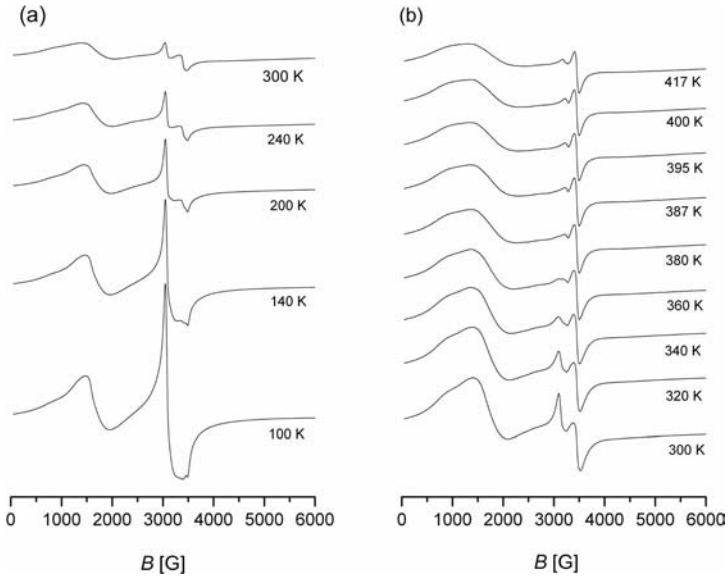

Figure 6. The EPR spectra of the iron(III) complex **1** at a) low and at b) high temperatures.

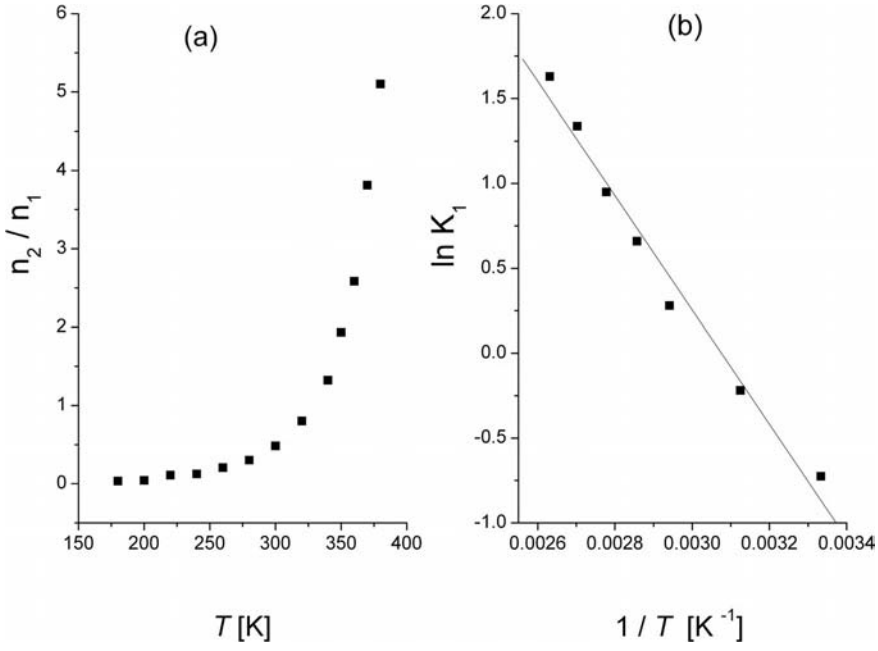

Figure 7. a) The temperature dependence of changing the number of the second-type of LS centers with respect to the first-type of LS centers for complex **1**; b) $\ln K_1$ vs. $1/T$. The solid line was calculated by means of Equation (4).

(n_1) with temperature increase by using numerical double integration of the corresponding parts of the spectrum (Figure 7, a).

Before considering this dynamic effect, the determination of the ground states for the LS centers of complex **1**, **2**, and **3** will be examined. The theory of the g tensors of LS d^5 (t_{2g}^5) systems in distorted octahedral environments was developed by Bleaney and O'Brien,[30] discussed by Griffith,[31] and applied to a large number of LS complexes.[5,22–25] The d^5 system is treated as a d^1 system via the hole formalism. Under the combined action of axial (Δ), rhombic (V) ligand-field distortions, and the spin-orbit interaction (λ), the sixfold degeneracy of the $^2T_2$ (t_{2g}^5) state is converted into three well-separated Kramers' doublets. The lowest Kramers' doublet in which resonance is observed has the form of Equation (5), where ψ_1 and ψ_2 are linear combinations of the 3d atomic orbitals associated with the t_{2g} level.

 © 2011 Wiley-VCH Verlag GmbH & Co. KGaA, Weinheim

$$\psi_1 = A\left|+1^+\right\rangle + B\left|\xi^-\right\rangle + C\left|-1^+\right\rangle,$$
$$\psi_2 = A\left|-1^-\right\rangle - B\left|\xi^+\right\rangle + C\left|+1^-\right\rangle \quad (5)$$

$$\xi = id_{xy} = (\left|+2\right\rangle - \left|-2\right\rangle)/\sqrt{2}; d_{xz} = -(\left|+1\right\rangle - \left|-1\right\rangle)/\sqrt{2};$$

$$d_{yz} = i(\left|+1\right\rangle + \left|-1\right\rangle)/\sqrt{2}$$

From the first-order interaction of these states with the magnetic moment operator ($k\boldsymbol{L} + g_e\boldsymbol{S}$) the expressions (6) for the principal g values are obtained; k is the orbital reduction factor.

$$g_z = -2[A^2 - B^2 + C^2 + k(A^2 - C^2)],$$
$$g_x = 2[2AC - B^2 + kB\sqrt{2}(C - A)],$$
$$g_y = -2[2AC + B^2 + kB\sqrt{2}(C + A)], \quad (6)$$
$$A^2 + B^2 + C^2 = 1$$

This parameter, as a rule, should be in the range of $0.7 \leq k \leq 1.0$, and it is regarded as a measure of the covalency of the metal-to-ligand bonds. The knowledge of the g values enables these equations to be solved for coefficients A, B, C, and k. The energy values (E_i) of the three Kramers' doublets, the axial (Δ) and rhombic (V) distortions are then found from the secular Equation (7) in the units of the spin-orbit coupling constant (λ).

$$\begin{vmatrix} -\lambda/2 + \Delta - E & -\frac{\lambda}{\sqrt{2}} & -3V \\ -\frac{\lambda}{\sqrt{2}} & -2\Delta - E & 0 \\ -3V & 0 & \lambda/2 + \Delta - E \end{vmatrix} = 0 \quad (7)$$

The paramagnetic resonance measurements give only the absolute principal g values, so that neither their signs nor the correspondence of g_1, g_2, or g_3 to g_x, g_y, or g_z are known. Thus, in a common case, one must consider 48 possible combinations depending on the labeling (x, y, z) and the signs chosen for the experimental results.

A home-written program was used for all these calculations. The experimental g values were fed into the program and generated all of the possible combinations. For each set, a solution to Equation (6) for A, B, C, and k was attempted using the Newton–Raphson method. As soon as the solution was obtained, the secular Equation (7) was solved. After matrix diagonalization, the solution was checked for its correspondence to the lowest Kramers' doublet. The best fit was selected on the basis of physically reasonable values for k, Δ, and V.

The calculated parameters obtained using the above theory are listed in Table 1, where the assigned g values, A, B, C, k coefficients, ligand-field distortions, and the relative energies of the ground and two excited Kramers' doublets are given. It is necessary to note that only one acceptable solution exists for all of the studied Fe^{III} complexes and the different types of LS centers of complex **1**. For the sake of comparison, the analogous parameters are listed in Table 1 for the bis(tridentate) iron(III) complex, $Fe[L]_2PF_6$, with PF_6^- as the counterion.[36]

In Table 1 all of the iron complexes (except for LS complex **1** of the second-type) have a very large B value, which indicates that the ground-state Kramers' doublet is characterized by the state where the unpaired electron resides in the d_{xy} orbital, thus $(d_{xz},d_{yz})^4(d_{xy})^1$ is the ground state. The situation is cardinally changed for the second-type of LS complex **1**. By utilizing the same axis definition, we determined $g_x = 1.975$, $g_y = -1.98$, and $g_z = -2.165$, which lead to the calculated axial (tetragonal) distortion of $\Delta/\lambda = -5.506$. The negative sign indicates that the d_{xy} orbital is higher in energy than the d_{xz} and the d_{yz} orbitals. The calculated coefficients A, B, and C also indicate that the unpaired electron is localized in the $(d_{xz} \pm d_{yz})$ orbital, and thus that the $(d_{xy})^2(d_{xz},d_{yz})^3$ ground state is stabilized. It should be noted that the change between the ground states is reversible with temperature.

The possibility of the two electron configurations $(d_{xy})^2(d_{xz},d_{yz})^3$ and $(d_{xz},d_{yz})^4(d_{xy})^1$ (as shown in Scheme 2) for low-spin Fe^{III} has previously been reported for several (porphinato)iron(III) complexes, $[TMPFe(L)_2]^+$.[32] But the change between the ground state in these LS iron(III) complexes was caused by changing the basicity of the pyridine axial ligands: the $(d_{xy})^2(d_{xz},d_{yz})^3$ configuration was realized for the high-basicity pyridines and the $(d_{xz},d_{yz})^4(d_{xy})^1$ configuration for the low-basicity pyridines. The conversion between the $(d_{xz},d_{yz})^4(d_{xy})^1/(d_{xy})^2(d_{xz},d_{yz})^3$ configurations in a single material, namely LS iron(III) complex **1**, was observed for the first time.

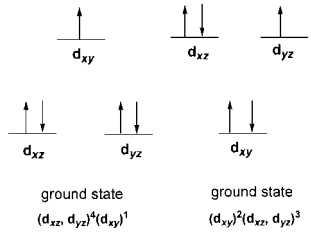

Scheme 2. Two possible electron configurations for the low-spin Fe^{III} centers.

The dynamic process involved in changing the number of the two different types of LS centers with temperature, as illustrated in Figure 7 (a), will now be explored. The temperature dependence of increasing the number of the second-type of LS centers (n_2) from the first-type of LS centers (n_1) can be characterized by the equilibrium constant K_1 and described by Equation (4). The enthalpy (ΔH_1) and entropy (ΔS_1) of this dynamic process, $\Delta H_1 = 27.9$ kJ/mol and $\Delta S_1 = 0.086$ kJ/mol, were calculated from the straight line given by plotting $\ln K_1$ vs. $1/T$ in the temperature range of 300 to 360 K (Figure 7, b). The enthalpy value obtained is close to the activation energy $E_a = 28.8$ kJ/mol that was found for the reorientation of the PF_6^- ion in the polycrystalline $NaPF_6$ compound,[33] which was determined from the temperature dependence of the spin-lattice relaxation time T_1. The comparison between these energies is possible

 © 2011 Wiley-VCH Verlag GmbH & Co. KGaA, Weinheim

because the chemical bond in both $NaPF_6$ and between Fe^{III} and PF_6^- in complex **1** is ionic. Thus, we postulated that the conversion between the $(d_{xz},d_{yz})^4(d_{xy})^1/(d_{xy})^2$-$(d_{xz},d_{yz})^3$ configurations is most probably caused by the reorientation of one coordinated PF_6^- ion from the equatorial (ONN) planar position to the axial one, which was previously occupied by water.

The EPR spectrum for complex **1** exhibited the appearance of the second-type of HS centers: a low-field broad line (600 G) with an effective g value of $g_2 \approx 5.6$ and a very broad unresolved signal in the $g \approx 2$ region (see Figure 6). This spectrum was analyzed by the rhombogram method[21,34,35] and indicated that the observed HS signals arise from the middle Kramers doublet when the crystal field parameters are $D > 0.3$ cm^{-1} and $E/D \approx 0.1$. It is interesting to note that the intensity of each type of LS and HS center changes synchronously: at low temperature the first-type predominates (LS center with $g_{x,y} = 2.215$, $g_z = 1.935$, and HS center with $D > 0.3$ cm^{-1}; $E/D \approx 0.3$), whereas at high temperature the second-type predominates (LS with $g_x = 1.975$, $g_y = 1.98$, $g_z = 2.165$, and HS with $D > 0.3$ cm^{-1}; $E/D \approx 0.1$). This synchronous behavior additionally confirmed the dimeric structure of complex **1** where the type of iron dimer is determined by the nature and location of the bridging units (H_2O or PF_6^-) between the LS and the HS centers. The proposed dimeric structure of complex **1** is schematically represented in Scheme 3.

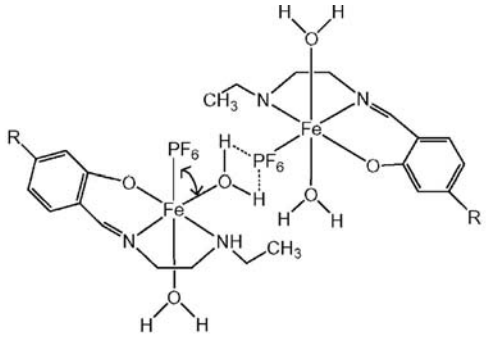

Scheme 3. Schematic representation of the proposed dimeric structure for iron(III) complex **1**.

Mössbauer Spectra for Complex 1

In order to confirm the EPR results, complex **1** was investigated by Mössbauer spectroscopy. Mössbauer quadrupole splitting can also be used to gain information concerning the electronic ground states. The gamma-resonance spectrum obtained at 297 K (Figure 8) is a superposition of two broad quadrupole doublets. The more intense doublet **1** (with an isomer shift of $\delta = 0.34$ mm/s with respect to α-Fe and with quadrupole splitting of $|\Delta E_Q| = 0.82$ mm/s) has parameters associated with the low-spin ($S = 1/2$) state of the Fe^{III} ion in an octahedral environment. Doublet **2** has parameters ($\delta = 0.28$ mm/s and $|\Delta E_Q| = 0.27$ mm/s) that correspond to the high-spin ($S = 5/2$) state of Fe^{III} in an octahedral environment.

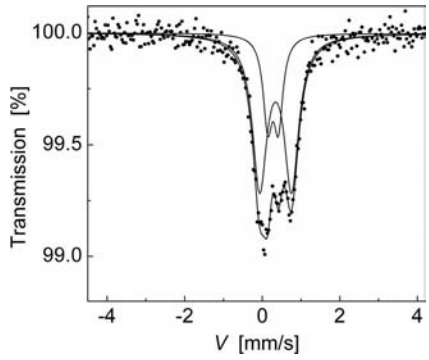

Figure 8. The Mössbauer spectrum for complex **1** recorded at 297 K.

At a temperature of approximately 80 K, the form of the transmission spectrum lines indicated the start of the magnetic phase transition in the sample (Figure 9).

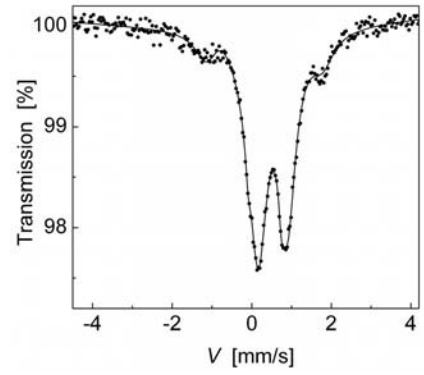

Figure 9. The Mössbauer spectrum for complex **1** recorded at 80 K.

The four nonequivalent positions of the ^{57}Fe atoms were detected in the experimental spectrum at 5 K (Figure 10, f). Two of the positions for the LS Fe^{III} centers gave two doublets that were characterized by the following parameters: $\delta = 1.18$ mm/s, $|\Delta E_Q| = 1.2$ mm/s (Figure 10, a) and $\delta = 0.8$ mm/s, $|\Delta E_Q| = 1.75$ mm/s (Figure 10, b), respectively. Two of the HS Fe^{III} centers showed magnetic hyperfine structure with the following parameters: Zeeman sextet with $\delta = 0.53$ mm/s, $\Delta E_Q < 0.02$ mm/s, and $H_{hf} = 519.2$ kOe (Figure 10, c) and a typical superparamagnetic line shape for metallocomplexes with dynamics in the magnetic subsystem[37,38] $\delta = 0.57$ mm/s, $\Delta E_Q = -0.18$ mm/s, and $H_{obs} = 456.4$ kOe (Figure 10, e). Curve e in Figure 10 was obtained by subtraction of the superposition curve, d = a + b + c, from the experimental spectrum (Figure 10, f). As the system progressed from a "slow" to a "fast" intramolecular dynamic process as the temperature increased, two of the LS and two of the HS parameters began to merge and a reduction in the number of nonequivalent positions from four at 5 K to two at 297 K was observed. The averaged quadrupole splitting for the LS centers of the Fe^{III} ion was ca. 1.47 mm/s.

 © 2011 Wiley-VCH Verlag GmbH & Co. KGaA, Weinheim

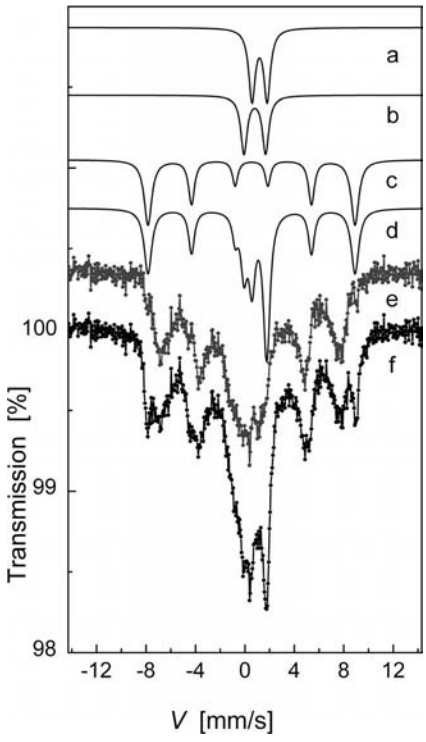

Figure 10. The experimental Mössbauer spectrum for complex **1** taken at 5 K (f). The solid curves (a, b, c, and d), which are located above the experimental spectrum, show the two LS and two HS iron(III) centers contributions (see text).

The same dynamic process was registered by both EPR and Mössbauer spectroscopy but over different time scales: the time scale for the Mössbauer spectroscopy was 10^{-7} s, whereas the time scale for the EPR spectroscopy was 10^{-9} s. Thus, the result of the thermo-stimulated intramolecular dynamics, which lead to the appearance of the time-dependent contributions in Hamiltonian of the hyperfine interactions, became visible only during the Mössbauer time frame and was observed at lower temperatures than in the EPR spectra.

The magnitude of the quadrupole splitting for the low-spin state is related to the electronic asymmetry about the ^{57}Fe nucleus. The electric field gradient QV_{ZZ} and the asymmetry parameter η are given by Equation (8).[39]

$$QV_{ZZ}/4 = (A^2/2 + B^2/2 - C^2)(1.5mm/s)$$
$$\eta = (V_{XX} - V_{YY})/V_{ZZ} = -(3/2)(A^2 - B^2)/(A^2/2 + B^2/2 - C^2) \quad (8)$$

A, B, and C are the orbital coefficients defined above. The quadrupole splitting was determined by Equation (9).[40]

$$\Delta E_Q = (QV_{ZZ}/2)(1 + \eta^2/3)^{1/2} \quad (9)$$

If the A, B, and C coefficients are known from the EPR results, we can calculate the quadrupole splitting. From the orbital coefficients given in Table 1, Equations (8) and (9) give ΔE_{Q1} = –1.40 mm/s and ΔE_{Q2} = 0.75 mm/s for the LS iron(III) centers of the first- and second-type, respectively. The calculated and observed values for the quadrupole splittings at low ($|\Delta E_Q|$ = 1.47 mm/s) and room ($|\Delta E_Q|$ = 0.82 mm/s) temperature were in agreement.

Thus, the Mössbauer data confirm the existence of the conversion effect of the electron configurations $(d_{xz},d_{yz})^4$-$(d_{xy})^1/(d_{xy})^2(d_{xz},d_{yz})^3$ on the basis of the quadrupole splitting values.

Conclusions

EPR and Mössbauer spectroscopy were successfully applied to determine the structure, magnetic, and dynamic properties of the liquid crystalline iron(III) Schiff base complexes with the asymmetric ligands. The six-coordinated Fe^{III} complexes, formed by coordination of the three ligator (ONN) atoms of the tridentate ligand (L), the water molecules and the different counterions [PF_6^- (**1**), NO_3^- (**2**), and Cl^- (**3**)], were studied for the first time.

It was shown that all of the complexes investigated consist of low-spin (LS) and high-spin (HS) iron centers. The orienting effect of a liquid crystalline matrix, and theoretical analysis of the observed g values were used in order to determine the direction of the principal (magnetic) g axes with respect to the molecular symmetry axes, the axial and rhombic field parameters and the relative energies of the exited and the ground states in the LS iron(III) complexes. It was determined that LS iron complexes **2**, **3** and LS complex **1** in the temperature range 4.2–250 K have a $(d_{xz},d_{yz})^4$-$(d_{xy})^1$ ground state.

Polycrystalline monocationic Fe^{III} complex [Fe(L)X-$(H_2O)_2]^+X^-$ (**1**) with X = PF_6^- as the counterion, has some interesting and important features. EPR spectroscopy showed that the LS and the HS centers are coupled together in **1** and form a dimer structure by means of the water molecules and the PF_6^- counterion. The appearance of the second-type of LS and HS iron centers was visible by means of EPR spectroscopy above room temperature. This type of iron center was best observed in the liquid crystalline (387–405 K) phase. The investigation of the dynamics of the appearance of the second-type of iron center showed that they arise due to the reorientation of the PF_6^- counterion in the dimer from the equatorial (ONN) planar position to the axial one, which was previously occupied by water. Theoretical analysis of the g values of the second-type of LS complexes demonstrated that in this case $(d_{xy})^2$-$(d_{xz},d_{yz})^3$ is the ground state. Conversion between the $(d_{xz},d_{yz})^4(d_{xy})^1/(d_{xy})^2(d_{xz},d_{yz})^3$ ground states is reversible with temperature. The observed conversion took place in a single material and was detected in the iron(III) complexes for the first time. It was also shown that the type of iron dimer is determined by the type and arrangement of the bridging units (H_2O or PF_6^-) between the LS and the HS iron centers.

Thus, we have synthesized for the first time a novel compound that has a labile LS electron configuration that switches between the $(d_{xz},d_{yz})^4(d_{xy})^1/(d_{xy})^2(d_{xz},d_{yz})^3$ ground states and is temperature dependent. Mössbauer data con-

 © 2011 Wiley-VCH Verlag GmbH & Co. KGaA, Weinheim

firmed the existence of such an effect on the basis of the values of the quadrupole splitting for the electron configurations $(d_{xz},d_{yz})^4(d_{xy})^1$ and $(d_{xy})^2(d_{xz},d_{yz})^3$.

Experimental Section

General: The preparation of the compounds **1**, **2**, and **3** has been described previously.[19] All the complexes were characterized by thin-layer chromatography, elemental analysis, IR, and NMR spectroscopy.[19] The LC properties were studied by differential scanning calorimetry.[19] The phase-transition temperatures and the corresponding transition enthalpies for the LC compounds are available in the Supporting Information. The presence of the complex-forming ion was confirmed by FTIR spectra in the far region.[20] The structure of the compounds was established with matrix-assisted laser desorption/ionization time of flight (MALDI-TOF).

The EPR experiments were carried out on powder samples and an anisotropic solution. The latter was prepared by dissolving the iron(III) complex in a eutectic mixture of a nematic liquid crystal N-8. The X-band (9.47 GHz) EPR measurements were performed with a CW-EPR EMXplus Bruker spectrometer that was provided with the helium ER 4112HV and the digital ER 4131VT temperature control systems. The standard ER 218G1 goniometer and high-quality quartz EPR tubes were used as well. The magnetic field was frequency modulated with 100 kHz so that the EPR spectra were recorded as first derivatives. At different temperatures, the microwave power was chosen such that saturation could be avoided. The accuracy of the reported magnetic parameters for the LS iron complexes was $\Delta g = \pm 0.005$. The orientation of the iron(III) complex in the nematic liquid crystal N-8 was investigated using the EPR spectrometer. The sample was kept in the resonator at room temperature in the presence of a high magnetic field (B_0 = 8000 G) for 5 to 10 min and then sharply cooled to low temperature while maintaining that field. In order to investigate the angular dependencies of the sample in the EPR spectra, the standard ER 218G1 goniometer was used, which allowed the sample to be rotated in one plane. The simulations of the EPR spectra were performed using home-made programs.

All of the Mössbauer spectra were obtained using a conventional constant-acceleration spectrometer where ^{57}Co in Cr matrix was used as the source. The velocity calibration was obtained by using the α-Fe spectrum. The isomer shift data were reported relative to the isomer shift of the α-Fe spectrum. A liquid nitrogen continuous-flow cryostat was used for the temperature measurements in the range of 80–300 K. The lower temperature measurements were made using a helium cryostat. The Mössbauer absorber, which was prepared as a thin layer of powder between two mylar discs, was mounted on the copper sample holder of the helium cryostat. The temperature measurements and control were carried out by a type-T thermocouple and a heater above 50 K with an accuracy of 1 K. A carbon-resistance thermometer, calibrated at the liquid nitrogen and liquid helium temperatures, was used for the temperature measurements and control below 50 K with an accuracy of 0.5 K.

Supporting Information (see footnote on the first page of this article): Synthesis and characterization methods for the iron complexes, differential scanning calorimetry results, and data of the elemental analysis.

Acknowledgments

The authors would like to thank Dr. Y. G. Gorbunova for her assistance with the MALDI-TOF-MS measurements, Dr. V. N. Konstantinov for supplying the program for the calculation of the EPR spectra of the orientationally ordered system, and Dr. R. T. Galeev for the superposition spectra calculation program. We thank Dr. V. G. Shtyrlin for the useful discussions. This research was supported by the President of the Russian Federation, grant number MK-1625.2009.3.

[1] Y. Maeda, N. Tsutsumi, Y. Takashima, *Inorg. Chem.* **1984**, *23*, 2440–2447.
[2] W. D. Federer, D. N. Hendrickson, *Inorg. Chem.* **1984**, *23*, 3861–3870.
[3] W. D. Federer, D. N. Hendrickson, *Inorg. Chem.* **1984**, *23*, 3870–3877.
[4] M. D. Timken, C. E. Strouse, S. M. Soltis, S. A. Daverio, D. N. Hendrickson, A. M. Abdel-Mawgoud, S. R. Wilson, *J. Am. Chem. Soc.* **1986**, *108*, 395–402.
[5] M. S. Haddad, M. W. Lynch, W. D. Federer, D. N. Hendrickson, *Inorg. Chem.* **1981**, *20*, 123–131.
[6] M. S. Haddad, W. D. Federer, M. W. Lynch, D. N. Hendrickson, *Inorg. Chem.* **1981**, *20*, 131–139.
[7] M. D. Timken, A. M. Abdel-Mawgoud, D. N. Hendrickson, *Inorg. Chem.* **1986**, *25*, 160–164.
[8] M. D. Timken, D. N. Hendrickson, E. Sinn, *Inorg. Chem.* **1985**, *24*, 3947–3955.
[9] R. Kannappan, S. Tanase, I. Mutikainen, U. Turpeinen, J. Reedijk, *Polyhedron* **2006**, *25*, 1646–1654.
[10] V. K. Sivasubramanian, M. Ganesan, S. Rajagopal, R. Ramaraj, *J. Org. Chem.* **2002**, *67*, 1506–1514.
[11] H. Fujii, T. Kurahashi, T. Ogura, *J. Inorg. Biochem.* **2003**, *96*, 133.
[12] L. Canali, D. C. Sherrington, *Chem. Soc. Rev.* **1999**, *28*, 85–93.
[13] A. Bottcher, E. R. Birnbaum, M. W. Day, H. B. Gray, M. W. Grinstaff, J. A. Labinger, *J. Mol. Catal. A – Chem.* **1997**, *117*, 229–242.
[14] A. Bottcher, M. W. Grinstaff, J. A. Labinger, H. B. Gray, *J. Mol. Catal. A – Chem.* **1996**, *113*, 191–200.
[15] L. Salmon, A. Bousseksou, B. Donnadieu, J. P. Tuchagues, *Inorg. Chem.* **2005**, *44*, 1763–1773.
[16] Yu. Galyametdinov, V. Ksenofontov, A. Prosvirin, I. Ovchinnikov, G. Ivanova, P. Gutlich, W. Haase, *Angew. Chem.* **2001**, *113*, 4399; *Angew. Chem. Int. Ed.* **2001**, *40*, 4269–4271.
[17] I. V. Ovchinnikov, T. A. Ivanova, V. E. Petrashen, Yu. G. Galyametdinov, G. I. Ivanova, *Appl. Magn. Reson.* **2005**, *29*, 325–334.
[18] V. M. Leovac, V. S. Jevtovic, L. S. Jovanovic, G. A. Bogdanovic, *J. Serb. Chem. Soc.* **2005**, *70*, 393–422.
[19] U. V. Chervonova, M. S. Gruzdev, A. M. Kolker, N. G. Manin, N. E. Domracheva, *Russ. J. Gen. Chem.* **2010**, *80*, 1643–1651.
[20] M. S. Gruzdev, U. V. Chervonova, A. M. Kolker, N. E. Domracheva, *Rus. J. Str. Chem.* **2011**, *52*, 88–95.
[21] R. Aasa, *J. Chem. Phys.* **1970**, *52*, 3919–3930.
[22] R. E. DeSimone, *J. Am. Chem. Soc.* **1973**, *95*, 6238–6244.
[23] T. L. Bohan, *J. Magn. Reson.* **1977**, *26*, 109–118.
[24] a) R. Rickards, C. E. Johnson, H. A. O. Hill, *J. Chem. Phys.* **1970**, *53*, 3118–3120; b) N. Domracheva, A. Mirea, M. Schwoerer, L. Torre-Lorente, G. Lattermann, *ChemPhysChem* **2006**, *7*, 2567–2577.
[25] N. E. Domracheva, S. A. Luchkina, I. V. Ovchinnikov, *Russ. J. Coord. Chem.* **1995**, *21*, 24–29.
[26] N. Domracheva, A. Mirea, M. Schwoerer, L. Torre-Lorente, G. Lattermann, *ChemPhysChem* **2005**, *6*, 110–119.
[27] I. V. Ovchinnikov, V. N. Konstantinov in *Radiospectroscopy of condensed matter* (Ed.: M. M. Zaripov), Nauka, Moscow, **1990**, pp. 90–110.

 © 2011 Wiley-VCH Verlag GmbH & Co. KGaA, Weinheim

[28] V. N. Konstantinov, I. V. Ovchinnikov, N. E. Domracheva, *Russ. J. Str. Chem.* **1984**, *25*, 19–27.
[29] M. R. A. Blomberg, P. E. M. Siegbahn, *Theor. Chem. Acc.* **1997**, *97*, 72–80.
[30] B. Bleaney, M. C. M. O'Brien, *Proc. Phys. Soc. London* **1956**, *69*, 1216–1231.
[31] J. S. Griffith, *The Theory of Transition Metal Ions*, Cambridge University Press, Cambridge, **1961**, p. 512.
[32] M. K. Safo, G. P. Gupta, C. T. Watson, U. Simonis, F. A. Walker, W. R. Scheidt, *J. Am. Chem. Soc.* **1992**, *114*, 7066–7075.
[33] H. S. Gutowsky, S. Albert, *J. Chem. Phys.* **1973**, *58*, 5446–5452.
[34] H. H. Wickman, M. P. Klein, D. A. Shirley, *J. Chem. Phys.* **1965**, *42*, 2113–2117.
[35] P. S. Rao, S. Subramanian, *Mol. Phys.* **1985**, *54*, 415–427.
[36] T. A. Ivanova, I. V. Ovchinnikov, A. N. Turanov, *Fiz. Tverd. Tela* **2007**, *49*, 2033–2038.
[37] J. L. Dormann, D. Fiorani, E. Tronc, *Adv. Chem. Phys.* **1997**, *98*, 283–494.
[38] I. M. Davletbaeva, A. V. Pyataev, K. E. Kalachev, E. K. Sadykov, R. A. Manapov, *Polym. Science Ser. A* **2006**, *48*, 612–617.
[39] G. Lang, W. Marshall, *Proc. Phys. Soc.* **1966**, *87*, 3–34.
[40] W. T. Oosterhuis, G. Lang, *Phys. Rev.* **1969**, *178*, 439–456.

Received: November 1, 2010
Published Online: January 31, 2011

 © 2011 Wiley-VCH Verlag GmbH & Co. KGaA, Weinheim